

Probe design for high-precision eddy-current displacement sensors

Vogel, Johan G.; Chaturvedi, Vikram; Nihtianov, Stoyan

DOI

[10.1109/IECON.2018.8591562](https://doi.org/10.1109/IECON.2018.8591562)

Publication date

2018

Document Version

Final published version

Published in

Proceedings

Citation (APA)

Vogel, J. G., Chaturvedi, V., & Nihtianov, S. (2018). Probe design for high-precision eddy-current displacement sensors. In M. Manic (Ed.), *Proceedings: IECON 2018 - 44th Annual Conference of the IEEE Industrial Electronics Society* (pp. 4877-4883). Article 8591562 IEEE. <https://doi.org/10.1109/IECON.2018.8591562>

Important note

To cite this publication, please use the final published version (if applicable). Please check the document version above.

Copyright

Other than for strictly personal use, it is not permitted to download, forward or distribute the text or part of it, without the consent of the author(s) and/or copyright holder(s), unless the work is under an open content license such as Creative Commons.

Takedown policy

Please contact us and provide details if you believe this document breaches copyrights. We will remove access to the work immediately and investigate your claim.

Probe Design for High-Precision Eddy-Current Displacement Sensors

Johan G. Vogel, Vikram Chaturvedi, Stoyan Nihtianov
Electronic Instrumentation Laboratory
Delft University of Technology
Delft, The Netherlands

Abstract—State-of-the-art industrial Eddy-Current Displacement Sensors (ECDSs) are typically not suitable for use in high-precision applications due to their low resolution and poor stability. By using a smaller, flat sensing coil, a reference coil, a dedicated readout chip and by operating at much higher excitation frequency a higher measurement sensitivity and better mechanical and thermal stability can be achieved. To use the sensor in industrial applications, the chip and the coils must be integrated in a small package. This paper presents a probe design for a high-precision ECDS, aiming at compactness and low thermal sensitivity. In this design, the sensing coil and the reference coil are closely spaced to minimise thermal gradients. The coils can, together with intermediate shielding and capacitive tilt electrodes, be integrated into a single stack only 2 mm thick and 12 mm in diameter, which can be realised on a multilayer PCB. Thermomechanical modelling shows that placing the readout chip on a separate PCB leads to significantly decreased self-heating compared to placement directly on the stack. Experiments show that the inductance behaviour of the realised stack is similar to that of the model.

Index Terms—eddy-current sensor, displacement measurement, probe design, coil inductance, self-heating.

I. INTRODUCTION

Displacement sensing at a resolution in the order of nanometres is of great importance in many high-precision applications such as lithography machines [1]. Numerous types of displacement sensors are available, all with their specific advantages and limitations [2, 3]. Laser interferometers, for example, have a large measurement range, but also require a large built-in space. Capacitive sensors, on the other hand, have a small measurement range, but are cost-effective and compact. Eddy-current sensors share these advantages of capacitive sensors, yet offer the additional benefit of being relatively insensitive to environmental parameters, such as fluctuations in humidity [4, 5].

Still, eddy-current sensors are not often used in high-precision applications, due to their low resolution and poor stability. State-of-the-art industrial eddy-current

sensors typically use large, wound coils with relatively poor stability and power hungry PCB-based electronics that is typically located far away and connected with long cables that introduce disturbances.

Nabavi et al. have introduced a novel architecture that enables to attain high sensitivity and thus high resolution [6]. An important improvement introduced by this novel architecture is the high excitation frequency of 20 MHz, which is much higher than state-of-the-art industrial eddy-current sensors, which operate at up to 2 MHz [7, 8]. This makes it possible to use flat, mechanically stable coils and to operate at a small standoff distance from the conductive measurement target, allowing for higher sensitivity. This eddy-current sensor makes use of two coils and is intended to perform differential measurements. Although differential operation improves sensitivity, in many applications only single-ended operation is feasible, as measurement targets are often large and are only accessible from a single side.

In our previous work, we developed a novel chip intended for single-ended operation that enables operation at an even higher frequency (>100 MHz) and smaller standoff (<100 μm). As a proof of concept, a prototype was developed that demonstrated a resolution of 1.85 nm for a 2 kHz bandwidth [9]. This prototype was intended as a proof-of-concept and all parts of the sensor were realised on a single PCB. However, this PCB is too large for use as a functional sensor, so that further miniaturisation and integration of all parts is required.

Conventional capacitive and eddy-current sensors typically have a cylindrical shape. Specifically for this ECDS, which operates at a small standoff, leading to increased sensitivity to tilt error [10], auto-alignment functionality is desirable. Thus, as the probe should fit into a Thermal Slider Actuator (TSA) [11], a diameter of 12 mm is required. Besides being compact, the sensor probe must also have a low thermal sensitivity, as the target resolution of the sensor is in the order of nanometres.

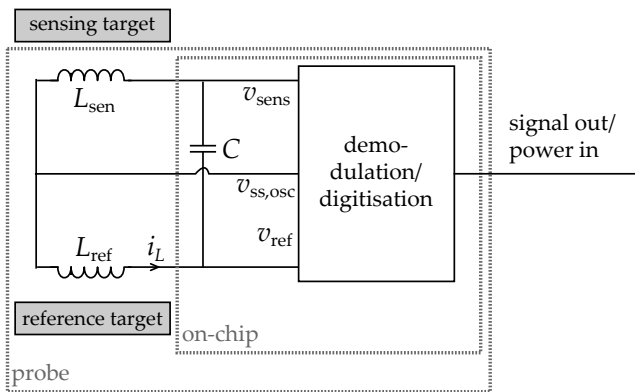


Figure 1: Equivalent circuit diagram of the single-ended ECDS system.

This paper presents the design of the compact probe and discusses the relevant design choices using finite element modelling and experiments. Section 2 introduces the architecture of the sensor and the two coils selected. Section 3 presents the design of the stack that contains the coils, supporting the critical geometry choices by Finite Element (FE) modelling. In Section 4 the placement of the readout chip is discussed in order to arrive at the final probe design. Section 5 compares experimental results of the manufactured coil stack with the FE results.

II. SENSOR ARCHITECTURE

Figure 1 shows the equivalent circuit diagram of the single-ended ECDS system. The circuit contains two coils, a sensing coil and a reference coil. The sensing coil faces the target for which the standoff distance needs to be measured. A change in the standoff distance leads to a change in the sensing coil inductance, which is measured by the electronics. As a measurement reference, a second coil is used, with an inductance equal to the nominal inductance of the sensing coil.

The two coils, together with an on-chip capacitor, form a resonator. An AC current with a frequency between 100 MHz to 200 MHz generates two voltages v_{sens} and v_{ref} , which are proportional to the coil inductances L_{sen} and L_{ref} . The high excitation frequency makes it possible to use relatively small, low inductance coils. This allows the use of flat coils, which have higher mechanical stability and higher measurement sensitivity, as the turns are closer to the measurement target.

The measurement value is obtained by dividing the difference of the inductance of the sensing coil and the reference coil by the inductance of the reference coil. This ratiometric measurement cancels multiplicative errors in the sensor and its readout, particularly in the excitation oscillator. In principle, the geometry of the reference coil could differ from that of the sensing coil. However, we decided to use a similar coil as the sensing coil and to keep the reference coil at a fixed standoff from a reference

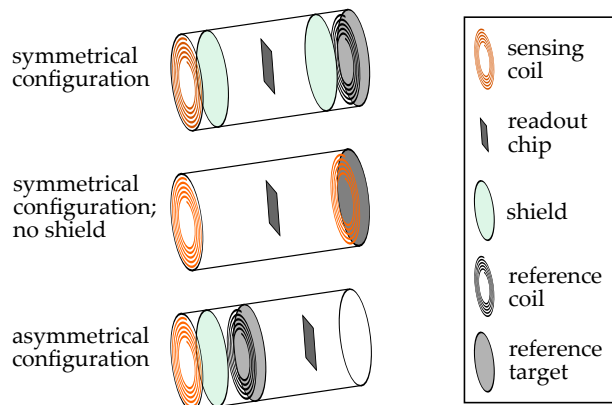


Figure 2: Configurations of the parts of the eddy-current sensor.

target, in order to improve symmetry and to partly cancel effects such as thermal expansion.

III. STACK DESIGN

A. Part configuration

The sensor probe should contain at least the two coils, the reference target and the electronic readout chip. These may be arranged in various ways, as is illustrated in Figure 2. A cylindrical housing shape has been chosen, as this is common for eddy-current sensors. The coils can be placed symmetrically or asymmetrically with respect to the readout chip. A reference target must be placed near the reference coil.

To minimise the interaction between the coils by mutual inductance, a shield can be used. In the symmetrical configuration, the coils are placed relatively far from each other, so that a shield may be omitted. In the asymmetric configuration a shield is necessary to prevent the coils from interacting. The asymmetrical configuration offers important advantages over the symmetrical configuration. Firstly, the coils can be placed on a single substrate, improving the stability of the connections to the readout chip. Secondly, they can be spaced more closely, so that they undergo more equal thermal expansion. In that way, the error due to thermal expansion is partly cancelled by the ratiometric principle.

As a carrier for the coils, the intermediate shield and the reference target, PCB material is used. PCB technology allows for rapid development of fully integrated, multilayer designs. The metal layers are normally copper with a common thickness of 35 μm . The high conductivity of copper ($\sigma = 58 \cdot 10^6 \text{ S/m}$), in combination with the high intended excitation frequency ($f = 200 \text{ MHz}$), leads to a small skin depth of $\delta = \sqrt{1/\pi\mu\sigma f} = 5 \mu\text{m}$, with $\mu = 4\pi \cdot 10^7 \text{ N/A}^2$ the magnetic permeability of copper. This is much smaller than the copper thickness, so that a copper layer will practically fully block magnetic fields, which is important for the use as a reference target or a shield.

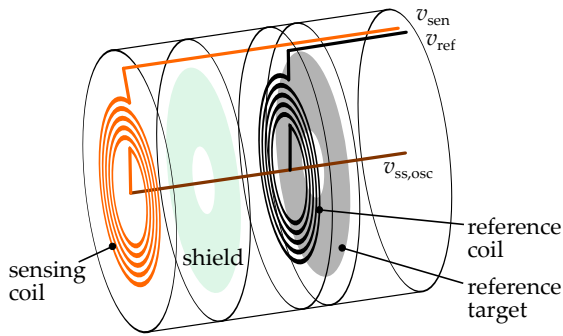


Figure 3: Layout of the coil stack including wiring.

Figure 3 shows the layout of the coil stack. The electrical connections of the coils are formed by vias that protrude up to the back surface of the stack. In the centre, the coils are connected to each other and to the virtual ground ($v_{ss,osc}$). On the outside, the coils are connected to v_{sen} and v_{ref} , respectively. As the vias run perpendicularly to the coil windings, the magnetic field of the coils is not disturbed by the vias. The vias to the outside of the coils (v_{sen} and v_{ref}) are placed close together in order to partly cancel their inductance.

B. Coil design

The readout chip requires the coils to have a nominal inductance of around 30 nH at a standoff of 100 μm , in order to generate an excitation signal of approximately ~ 200 MHz in combination with the on-chip capacitance of 10 pF. A compact seven-turn Archimedean coil with a nominal outer radius (i.e. average radius of the outer turn) of 2.2 mm and a trace width and trace spacing of 0.13 mm has been selected. The coils are manufactured on PCB, are made of copper and have a thickness of 35 μm . The measurement sensitivity found using FE modelling is 0.25 nH/ μm .

C. Reference target and shield design

1) *Reference target dimensions:* For the sake of symmetry, the reference coil was chosen to be equal to the sensing coil. Also the distance between the reference target and the reference coil is chosen to be equal to the sensor's nominal standoff. To prevent electrical contact with the common of the coils ($v_{ss,osc}$), the reference target should be a ring with a hole in the centre. Traditionally, the size of a target must, as a rule of thumb, be three to five times larger than the probe diameter [5]. The result in this case would be a large outer diameter, which is unfavourable. However, as the nominal standoff of this sensor is very small, it is expected that the target does not have to be much larger than the coil.

To find the required inner and outer diameter of the reference target, a 2D axisymmetric FE model was developed in Comsol using the magnetic fields toolbox.

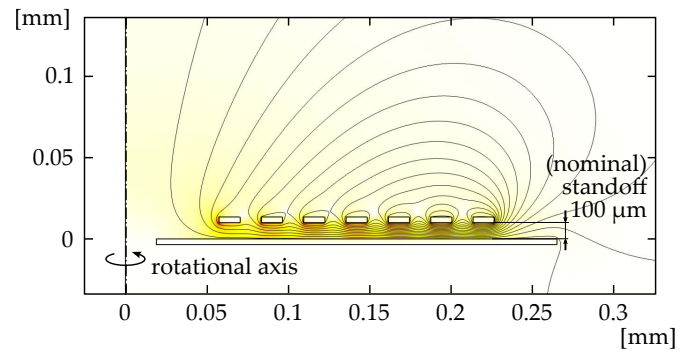


Figure 4: Cross-section of the coil in the 2D axisymmetric FE model to study the required target disk overlap u . Plotted are the magnetic field lines and the magnetic field density (in colour).

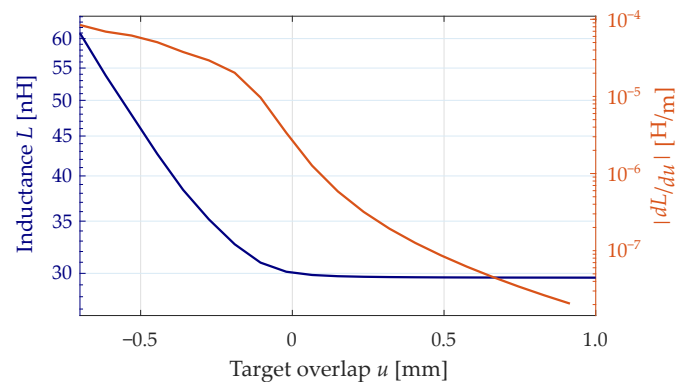
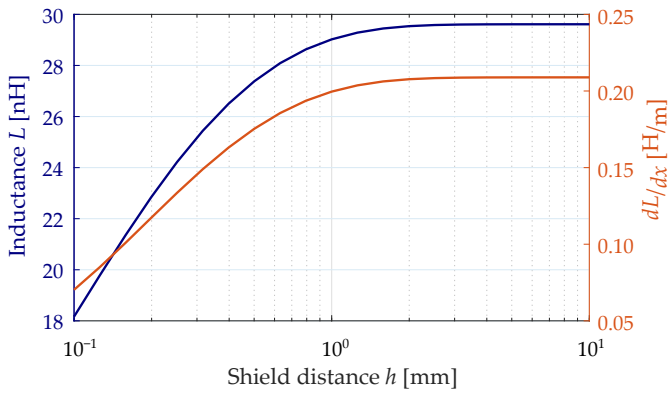


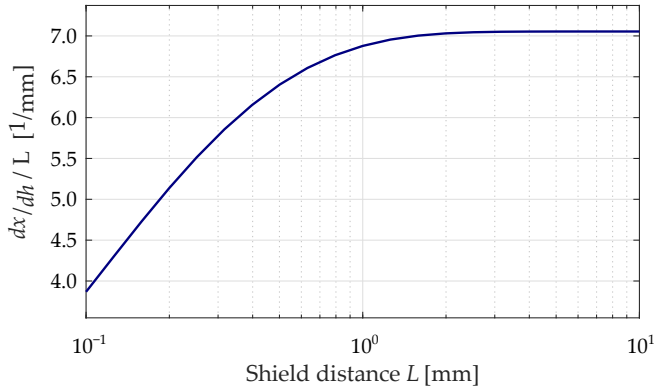
Figure 5: Reference coil inductance L (blue) as a function of the target disk overlap u and the related sensitivity $\partial L/\partial u$ (red).

Figure 4 shows the cross-section of the model with its boundary conditions. A 35-micrometre thick copper target was placed at a 100 μm distance from the coil turns. The inner and outer diameters of the target were set equal to the ones of the coil and were then varied such that the outer radius increased and the inner radius was reduced by a distance u ('overlap').

Figure 5 shows the coil inductance as function the reference target overlap u and its derivative $\partial L/\partial u$. The target size should be such that the inductance is close to the inductance of an infinite target. For additional space of 0.1 mm and over, the coil inductance is within 1 % of the infinite target inductance. Furthermore, even in the worst case scenario, i.e. only the reference target experiences thermal expansion, the inductance change should be negligible. Making use of a thermal expansion coefficient of $13 \cdot 10^{-6}$ 1/K of the PCB material FR4 and the measurement sensitivity $0.25 \cdot 10^{-3}$ H/m, a target size sensitivity of $8 \cdot 10^{-6}$ H/m would lead to an allowable thermal sensitivity of 1 nm/K. According to Figure 5, this corresponds to a required minimum overlap of $u = 0.0$ mm. In the final design, an overlap of 0.3 mm was used,



(a) Inductance L (blue) and measurement sensitivity $\partial L/\partial x$ (red).



(b) Normalised measurement sensitivity $1/L \cdot \partial L/\partial x$.

Figure 6: Sensing coil inductance and measurement sensitivity as function of the shield distance h .

both as a precaution and to account for the fact that the maximum radius of the spiral coil is somewhat larger than its nominal radius.

2) *Shield distance*: A shield is used between the coils to isolate their magnetic fields, so that the mutual inductance of the coils is low. In this way, the coils can still be placed close together, so that they experience similar thermomechanical conditions. The presence of the shield, however, should not deteriorate the measurement sensitivity of the coil too much.

Figure 6a shows the inductance and measurement sensitivity $\partial L/\partial x$ as a function of the shield distance h . Indeed, the sensitivity decreases with a smaller shield distance. However, as the inductance also decreases with a smaller h , the normalised measurement sensitivity, $1/L \cdot \partial L/\partial x$, decreases less quickly. Figure 6b shows the normalised measurement sensitivity. As a trade-off between distance and sensitivity loss, a distance between the coils and the shield of 0.540 mm has been selected.

3) *Shield dimensions*: Another important requirement is the mutual inductance of the coils, which should be much lower than the coil inductance for good isolation. Figure 7 shows the mutual inductance as a function of the shield overlap v compared to the inner and outer radii of the coil. The mutual inductance rapidly decreases

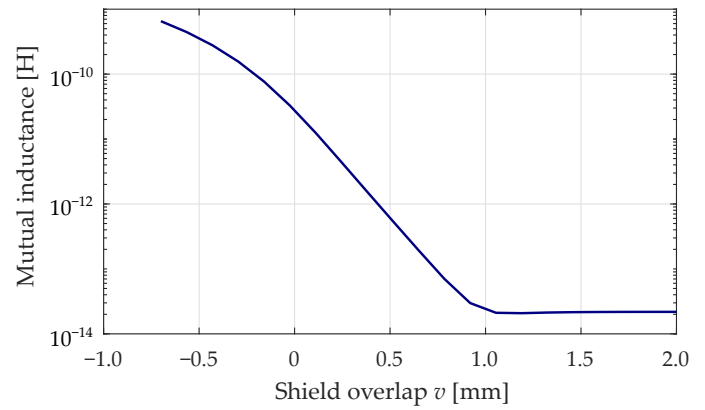


Figure 7: Mutual inductance of the coils as function of the shield overlap v .

with an increasing v . If an additional shield width of 0.3 mm is chosen, so that the shield has a similar geometry to the reference target, the mutual inductance will be very low (6.3 pH) compared to the nominal inductance of the coils (~ 30 nH).

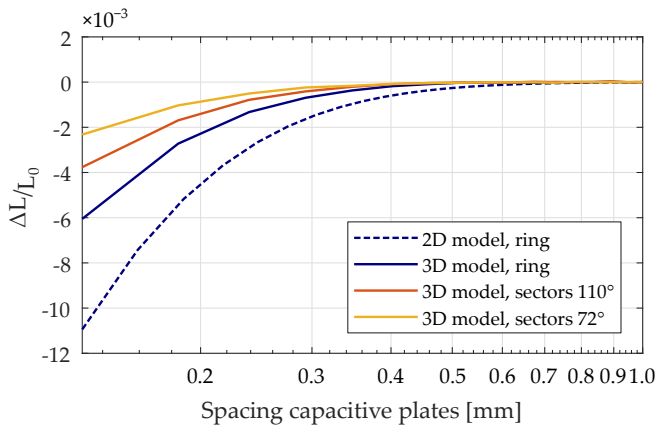
D. Capacitive electrodes

To attain a high measurement sensitivity, the ECDS is operated at small standoff distance (approx. 100 μm). At such a small standoff, however, the sensitivity to misalignment is significant [10]. To compensate for the misalignment, or to perform auto-alignment, the relative orientation of the probe with respect to the target should be measured. For this purpose, three capacitive electrodes are placed around the eddy-current coil. These electrodes measure the two tilt degrees of freedom and the standoff, independent from the measurement of the eddy-current sensor. Since tilt measurement does not require a high bandwidth nor a low gain error, capacitive measurement is a good candidate for this function.

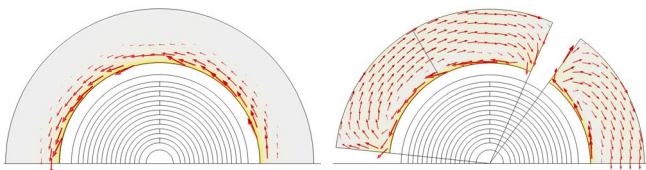
As the capacitive electrodes are conductive and are placed in the vicinity of the sensing coil, they should not significantly influence the inductance of the sensing coil. FE modelling was used to determine how close together the electrodes and the sensing coil can be spaced. First, the capacitive electrodes were modelled as a full 2.5-mm width ring, instead of separate sectors, using a 2D axisymmetric model based on the one of Figure 4.

Figure 8a shows the inductance change due to the presence of the capacitive ring. The change was normalised by dividing by the nominal coil inductance. The results show that for a 0.2-mm spacing around the coil, the inductance change is below 0.5 %.

A full ring is expected to have a larger influence on the inductance than do separate sectors. To discover how large the effect of separate sectors is in comparison to a full ring, a 3D FE model was used, which is much more computationally intensive than a 2D model. Figure 8a



(a) Inductance as function of the spacing between the sensing coil and the capacitive electrodes.



(b) Eddy-current flow in the ring electrode (left) and the sectored electrodes (right). The arrows are scaled logarithmically.

Figure 8: Effect of capacitive electrodes in the vicinity of the sensing coil.

shows that the change in inductance resulting from a ring electrode is in the 3D model almost a factor of two lower than in the 2D model. This could be due to the fact that in the 3D model the coil and the capacitive electrode are modelled as a layer with a mathematical thickness, whereas in the 2D model the thickness is implemented geometrically. The model, however, does show that sectored electrodes lead to a significantly less inductance change than a ring electrode.

Figure 8b compares the current flow of the eddy-currents in a ring electrode and sectored electrodes. Note that the arrow length is scaled logarithmically. In the sectored electrodes, the current flows along the inner radius, but must then go backwards, flowing relatively homogeneously through the rest of the surface.

In the final probe design, a distance of 0.5 mm was selected between the outer radius of the coil and the inner radius of the capacitive electrodes. This leads to a negligible change in inductance (smaller than 0.03 %). The outer diameter of the electrodes is 10.4 mm, so that the surface area is approximately 12.4 mm².

IV. PROBE DESIGN

A. Readout chip placement

The readout chip can be placed in various ways with respect to the coil stack. Figure 9 shows two possible configurations. Direct placement of the chip onto the

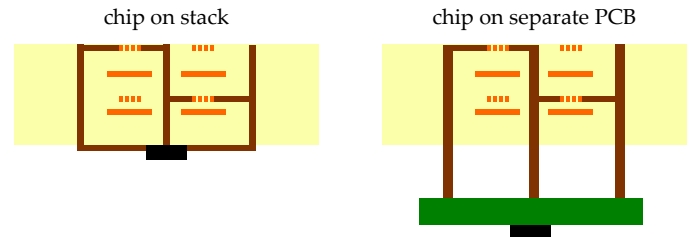


Figure 9: Possible configurations of the chip with respect to the coil stack.

stack (left configuration) is possible if the substrate allows electrical connection of the chip and the soldering of a few additional electronic components. In terms of the number of components, this is the simplest configuration. A further advantage is that the parasitic inductance of the coil wiring can be minimised.

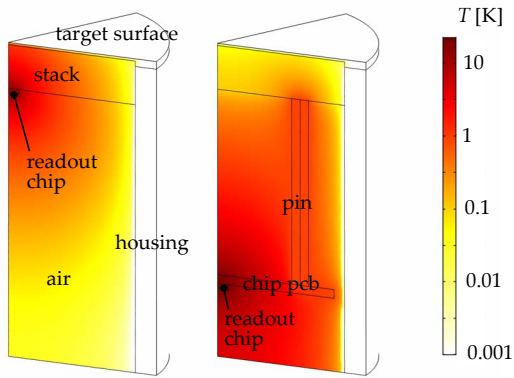
Alternatively, the readout chip and the electronic components can be placed on a separate PCB, which is connected with pins to the stack (right configuration). This configuration allows for modularity of the stack and readout electronics but requires longer connections to the coils, adding approximately 1 nH of parasitic inductance per millimetre of wire length. However, a major advantage of this configuration is the better thermal decoupling of the stack and the readout.

B. Thermomechanical analysis

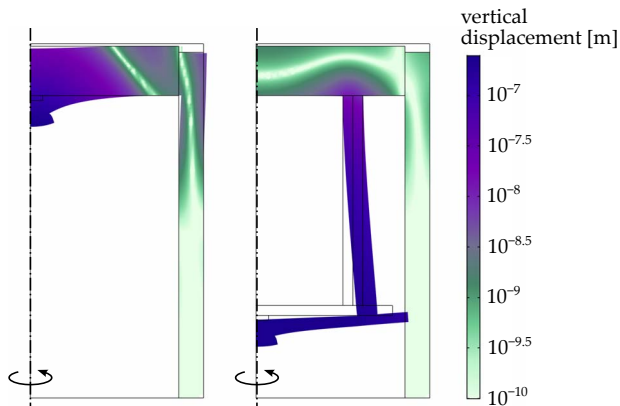
For a 10 mA excitation current through the coils, the amount of power dissipated in the coils is small, in the order of 0.2 mW. Most power, however, is dissipated by the readout chip, which consumes 9.1 mW [9]. To study the effect of the power dissipation in the readout chip, a 3D thermomechanical FE model was developed in Comsol. A one sixth probe sector was modelled in both configurations (Figure 10a). The coil stack was placed in an aluminium housing kept at room temperature and fixed in position at its bottom. The space inside the probe and in the gap between the stack and the target was filled with air. As the air volumes were relatively small, the main heat transport through the air was assumed to be diffusion.

Figure 10a shows the temperature rise with respect to the ambient temperature. The maximum temperature rise of the stack in the configuration with a separate readout PCB is 0.9 K, which is much lower than in the configuration without it (13 K). Figure 10b shows the (scaled) deformation shape resulting from the temperature distribution. In colour, the absolute value of the vertical displacement is shown. The maximum displacement within the stack in the configuration without a separate readout PCB is 200 nm and reduces in the configuration with the separate readout PCB to 13 nm.

The simulation results must be considered with care, as both the temperature and deformation change for



(a) Temperature rise with respect to the ambient.



(b) Deformed shape and, in colour, absolute displacement in the vertical direction.

Figure 10: Thermomechanical response of the eddy-current probe due to 9.1 mW heat dissipation in the readout chip.

different thermomechanical boundary conditions. In addition to that, the acceptable temperature change highly depends on the application, whereas deformation of the stack may to a certain extent be allowable, as long as it is static. The configuration with the separate readout PCB, however, is clearly superior to the other configuration. Further reduction of thermomechanical effects can be achieved by using copper wiring as alternative paths for removing the heat from the readout PCB, which is more effective in this configuration, due to the thermal resistance between the readout chip and the coil stack.

C. Final design

The coil stack (Figure 11) was manufactured using a six-layer PCB technology. At the back, it contains pads for soldering the pins that connect to the readout chip PCB. Figure 12 shows the design of the sensor probe, including the separate readout PCB. This probe can be inserted into a cylindrical housing by clamping the coil stack or applied in the Thermal Slider Actuator (TSA) [11]. The PCB with the readout chip is mechanically supported by the pins. The supply and signals of the

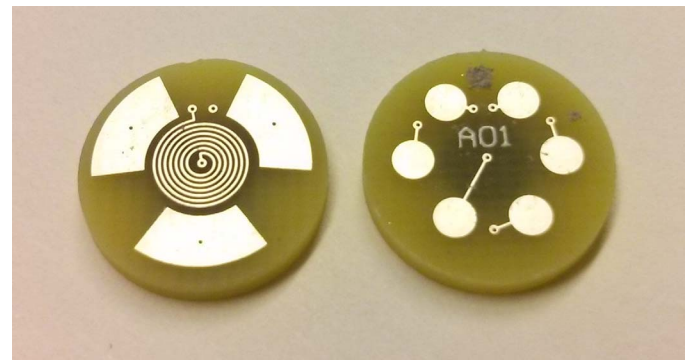


Figure 11: Picture of the coil stack.

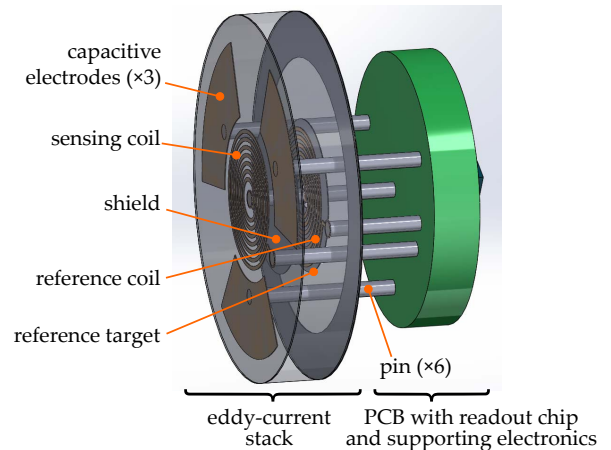


Figure 12: Final design of the sensor probe.

chip require cabling to the outside world. This cabling and some additional electronics to amplify the digital signals are the subject of future work, but these are no critical parts in the design of this sensor.

V. EXPERIMENTAL RESULTS

To verify performance, the inductance of the coils on the stack was measured without connecting the readout chip. This was done using an HP 4294A impedance analyser in combination with a 42941A impedance probe. The measurement was performed at 110 MHz – the highest frequency supported by the impedance analyser.

Figure 13 shows the inductance of the sensing and the reference coils as a function of the standoff. The dotted lines with the point marks are from the measurements; the solid lines from an axisymmetric FE model are similar to the one in Section III-C3. Note that an offset of 5.0 nH was added to the modelling results of both coils to better visualise to what extent the shape of the model and measurement results match.

Indeed, the shape of the measured sensing coil inductance is highly similar to the modelled one. At the

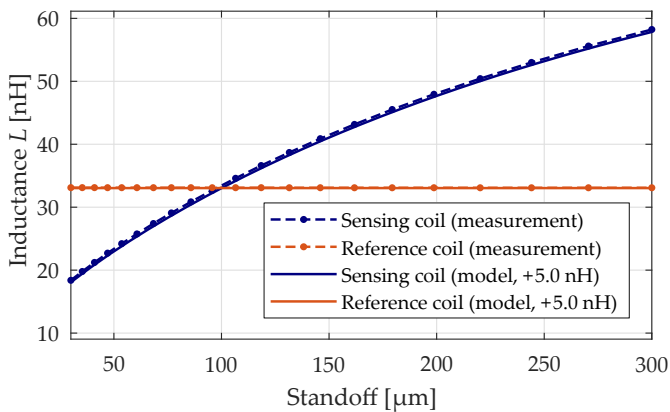


Figure 13: Inductance and sensitivity of the coils in the coil stack, both measured and modelled.

nominal standoff of 100 μm , the measured sensitivity $\partial L/\partial x$ is 0.176 nH/ μm , which is close to the 0.180 nH/ μm for the model. As expected, the inductance of the reference coil is constant (i.e. not affected by standoff change), both in the model and the measurement.

The sensing coil has, as intended, almost equal inductance as the reference coil at the nominal standoff of 100 μm , both in the measurement and the model.

The inductance offset of the measurement with respect to the model is almost equal for both coils (approximately 5.0 nH). This offset might be explained by the wiring of the coils, not modelled here, which leads to increased inductance, and calibration error of the impedance probe.

VI. CONCLUSION

In this paper, an ECDS probe design is proposed that integrates the chip, the sensing and reference coils and the reference target. The design has been optimised for compactness and low thermal sensitivity.

Placing the sensing coil and the reference coil closely together leads to better thermal stability of the probe. To prevent interaction between the coils, a shield layer is placed between the coils at distance of 540 μm . This distance leads to a moderate reduction of the measurement sensitivity (approximately 8 %). The reference target can be ring-shaped and needs to overlap the coil only slightly (0.3 mm) to have a negligible effect on the coil inductance and its sensitivity to thermal expansion.

A similar overlap of the shield leads to a mutual inductance of more than three orders smaller than the nominal coil inductance. Capacitive electrodes are placed around the sensing coil to facilitate tilt angle measurement. A distance of 0.5 mm is enough to negligibly affect the coil inductance.

The whole stack of sensing coil and capacitive electrodes, shield, reference coil and reference shield can be realised within a single substrate: the coil stack. This stack can be realised in a multilayer PCB of only 2-mm

thick and has, including capacitive electrodes, a diameter of 12 mm. The readout chip is placed on a separate PCB which is electrically and mechanically connected to the coil stack using pins. This strongly reduces the thermo-mechanical effects caused by the power dissipation in the chip, as compared to direct mounting of the chip on the stack.

Experiments show a good match between the modelled coil inductance and the one measured in a manufactured stack. Further work will involve the realisation and qualification of the full sensor probe including the readout chip.

REFERENCES

- [1] R.H. Munnig Schmidt. Ultra-precision engineering in lithographic exposure equipment for the semiconductor industry. *Philosophical Transactions of the Royal Society of London A: Mathematical, Physical and Engineering Sciences*, 370(1973):3950 – 72, 2012.
- [2] J. Shieh, J.E. Huber, N.A. Fleck, and M.F. Ashby. The selection of sensors. *Progress in Materials Science*, 46(3 – 4):461 – 504, 2001.
- [3] A.J. Fleming. A review of nanometer resolution position sensors: Operation and performance. *Sensors and Actuators A: Physical*, 190:106 – 126, 2013.
- [4] S. Nihtianov. Measuring in the subnanometer range: Capacitive and eddy current nanodisplacement sensors. *IEEE Industrial Electronics Magazine*, 8(1):6–15, March 2014.
- [5] Lion Precision. Differences between capacitive and eddy-current sensors. Technical report, 2013.
- [6] M.R. Nabavi, M.A.P. Pertijs, and S. Nihtianov. An interface for eddy-current displacement sensors with 15-bit resolution and 20 mhz excitation. *Solid-State Circuits, IEEE Journal of*, 48(11):2868 – 81, Nov. 2013.
- [7] Micro-Epsilon. *eddyNCDT // Eddy current sensors for displacement and position*. Micro-Epsilon.
- [8] Lion Precision. Minimum recommended eddy-current target thickness. Eddy-Current TechNote LT02-0011, Lion Precision, 2008.
- [9] V. Chaturvedi, J. G. Vogel, K. A. A. Makinwa, and S. Nihtianov. A 9.1 mw inductive displacement-to-digital converter with 1.85 nm resolution. In *2017 Symposium on VLSI Circuits*, pages C80–C81, June 2017.
- [10] J.G. Vogel and Stoyan Nihtianov. Tilt sensitivity of an eddy-current position sensor for high-precision applications. In *Proceedings of the 16th international conference of the EUSPEN*, pages 177 – 8, 2016.
- [11] O.S. van de Ven, J.G. Vogel, S. Xia, J.W. Spronck, and S. Nihtianov. Self-aligning and self-calibrating capacitive sensor system for displacement measurement in inaccessible industrial environments. *IEEE Transactions on Instrumentation and Measurement*, 67(2):350–358, Feb 2018.